Near-Infrared Gold Nanocages as a New Class of Tracers for Photoacoustic Sentinel Lymph Node Mapping on a Rat Model

Kwang Hyun Song, Chulhong Kim, Claire M. Cobley, Younan Xia,* and Lihong V. Wang*

Department of Biomedical Engineering, Washington University in St. Louis, St. Louis, Missouri 63130-4899

ABSTRACT

This work demonstrated the use of Au nanocages as a new class of lymph node tracers for noninvasive photoacoustic (PA) imaging of a sentinel lymph node (SLN). Current SLN mapping methods based on blue dye and/or nanometer-sized radioactive colloid injection are intraoperative due to the need for visual detection of the blue dye and low spatial resolution of Geiger counters in detecting radioactive colloids. Compared to the current methods, PA mapping based on Au nanocages shows a number of attractive features: noninvasiveness, strong optical absorption in the near-infrared region (for deep penetration), and the accumulation of Au nanocages with a higher concentration than the initial solution for the injection. In an animal model, these features allowed us to identify SLNs containing Au nanocages as deep as 33 mm below the skin surface with good contrast. Most importantly, compared to methylene blue Au nanocages can be easily bioconjugated with antibodies for targeting specific receptors, potentially eliminating the need for invasive axillary staging procedures in addition to providing noninvasive SLN mapping.

Nanoparticles have gained considerable attention for a number of biological and medical applications, ever since the discovery that they can be utilized efficiently for delivering[1,2] and targeting[3,4] therapeutic agents to a specific site. In addition to therapeutic procedures, nanoparticles are widely used for diagnostic purposes,[3,5,6] as they can be engineered to enhance the contrasts of imaging modalities such as optical imaging,[3,7,8] magnetic resonance imaging (MRI),[9–11] and computed tomography (CT).[12,13] Nanoparticles have widely tunable properties such as sizes, shapes, and compositions, so their application in imaging should be broad. In diagnosis, nanomaterials can be used to identify sentinel lymph nodes (SLNs) for axillary staging in breast cancer patients.

Sentinel lymph node biopsy (SLNB) is widely performed and has become the standard for axillary staging. In SLN mapping as a prerequisite for SLNB, a blue dye (e.g., isosulfan blue, or methylene blue) and/or nanometer-sized radioactive colloids (e.g., technetium-99 (^{99}mTc)) are usually used in the clinic.[14,15] However, these methods have several limitations: (1) The method using a blue dye requires a surgical operation to expose a SLN for visual detection and also necessitates some experienced hands. (2) This method often leaves a blue stain on the injection point in the skin for months after the surgery.[16] (3) The radioactive colloid method not only requires special facilities for handling radioactive isotope materials but also suffers from the low spatial resolution of Geiger counters for noninvasive SLN identification.[17] In addition, the method takes about 24 h for nodal uptake due to the large size of the tracers (typically 100–200 nm) and may cause radiation damage to the connective tissues of the skin. Therefore, noninvasive, nonionizing, and high-resolution mapping of SLNs would be beneficial to breast cancer patients, and would greatly aid minimally invasive staging methods such as fine needle aspiration biopsy (FNAB).[18]

MRI has been tried with an ultrasmall superparamagnetic iron oxide (USPIO, 17–20 μm[19]) contrast agent for SLN mapping.[20,21] Even though MRI provides an excellent imaging depth and spatial resolution, it still suffers from low sensitivity and high cost. Furthermore, patients need to be transported from an operating room to a MRI unit since most operating rooms do not have MRI capabilities. On the other hand, optical imaging has several orders of magnitude higher sensitivity than MRI and can be readily and easily adapted to the clinic.[17] Optical imaging is also nonionizing and relatively inexpensive. Therefore, optical lymph node tracers,

* Corresponding authors. E-mail: (L.V.W for photoacoustic imaging) lhwang@biomed.wustl.edu; (Y.X. for nanocages) xia@biomed.wustl.edu.

such as fluorescent beads[17] (20−200 nm) and quantum dots[7,22] (15−20 nm), have been studied for noninvasive SLN mapping based on fluorescent imaging. However, these methods have poor spatial resolution at depths beyond one transport mean free path (∼1 mm), resulting in inaccurate localization of SLNs since the average depth of SLNs is 12 ± 5 mm in humans (from the top surface of SLNs to the skin surface).[23] Moreover, the methods using quantum dots can create potential heavy metal toxicity in clinical use.[24]

Recently, the Wang group demonstrated PA SLN mapping using clinically available methylene blue.[25] PA imaging modality is an emerging hybrid technology that is highly sensitive to endogenous and exogenous optical contrasts and provides good ultrasonic spatial resolution. Since this imaging technique uses diffusive photons, it can achieve up to ∼50 mm imaging depth in biological tissues.[26] PA imaging for SLN mapping demonstrated a depth capability of ∼31 mm with satisfactory spatial resolution and clinical potential. However, methylene blue-based PA mapping poses potential challenges. For example, since the methylene blue molecule (0.7 nm in diameter and 1.6 nm in length) is smaller than 5 nm and easily flown into the echelon lymph nodes, there is a high possibility of false positives.[21,27] Methylene blue molecule is also difficult to be bioconjugated to form molecular probes with a targeting capability. Since typical breast tissues have higher optical absorption and scattering at the peak absorption wavelength of methylene blue (677 nm, PA excitation: 655 nm) than at the near-infrared (NIR) regions, it is hard to achieve relatively deep penetration depth.

In this study, for the first time to our knowledge, we apply NIR Au nanocages as a lymph node identifier to a noninvasive PA imaging modality. Au nanocages have attractive features such as biocompatibility, easy surface modification for targeting,[28,29] no potential heavy metal toxicity,[24] a broad range of sizes (35−100 nm), tuning of the localized surface plasmon resonance (LSPR) peak, strong optical absorption in the NIR region,[29,30] and encapsulated site-specific drug delivery.[31] In a rat model, we have successfully identified an in vivo SLN with enhanced contrast by Au nanocages and good spatial resolution noninvasively. In addition, we have demonstrated the depth capability of Au nanocages in SLN mapping as deep as ∼33 mm. We expect that non-invasive SLN mapping based on Au nanocages can be beneficial to breast cancer patients. Going forward, by employing surface-modified Au nanocages, which can bind to specific breast cancer cells, this technique may constitute a noninvasive means of SLNB.

Materials and Methods. *Au Nanocages.* Au nanocages are cubic nanoboxes with hollow interiors and porous walls (inset in Figure 1). They can be conveniently synthesized through a simple galvanic replacement reaction between Ag nanocubes and chloroauric acid ($HAuCl_4$) in water[31,32]

$$3Ag(s) + AuCl_4^-(aq) \rightarrow Au(s) + 3Ag^+(aq) + 4Cl^-(aq)$$

The Ag nanocubes were in turn prepared using a rapid, sulfide-mediated polyol process with poly(vinyl pyrrolidone) (PVP) serving as a capping agent. The LSPR peak of the Au nanocages was tuned to 735 nm by controlling the ratio
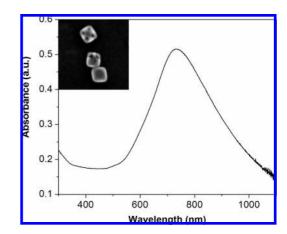
Figure 1. Absorption spectrum of Au nanocages. Wavelength at peak optical absorption was ∼735 nm. Inset shows a typical SEM image of the Au nanocages with the scale bar being 50 nm. The average edge length was 50.3 ± 6.7 nm (standard deviation). The Au nanocages were stabilized with polyvinyl pyrrolidone (PVP).

between Ag and $HAuCl_4$ (Figure 1). The average edge length of the Au nanocages used for this study was 50.3 ± 6.7 nm (standard deviation). The concentration of Au nanocages for the imaging study was 2 nM in water. The Au nanocages were stabilized with PVP.

Imaging System. A reflection-mode PA imaging system was employed for identifying SLNs following Au nanocage injection (see our previous work[33] for a detailed description of the system). For PA excitation, a pulsed laser system with 755 nm wavelength was employed. This wavelength was close to the optical absorption peak of the Au nanocages. The laser system has a 10 Hz pulse repetition frequency and a 10 ns pulse width. The laser light delivered to the skin was sufficiently broadened to conform to the maximum permissible exposure (MPE) limitation (actual fluence, 11 mJ/cm^2; MPE, 26 mJ/cm^2).[34] To detect PA waves with low acoustic attenuation, a 3.5 or a 5 MHz central frequency ultrasonic transducer (V380, V308, Panametrics-NDT) was used. Both transducers were spherically focused with 4.95 and 2.54 cm focal lengths; 2.54 and 1.91 cm diameter active elements; and 70 and 72% -6 dB round-trip bandwidths, respectively.

Phantoms. To estimate the concentration of Au nanocages accumulated in a SLN of a rat ex vivo, phantom experiments were performed. Phantoms were made of 12% porcine gelatin containing Au nanocages of various concentrations (0.1−8 nM). The phantoms (a cylinder with 3 mm in diameter and 4 mm in length) were made similarly in shape and size to a real SLN of a rat to rule out the effect of the size differences for PA signal measurement. PA signals were directly measured from these phantoms (Figure 3B). Similarly, PA signals from excised real SLNs were also measured in the same way and compared with those from the phantoms to estimate the concentrations of Au nanocages accumulated in SLNs.

Animals. Sprague−Dawley rats weighing 250−390 g were used. The rats were initially anesthetized with a mixture of Ketamine (85 mg/kg) and Xylazine (15 mg/kg). The region of interest was gently depilated using a commercial hair-
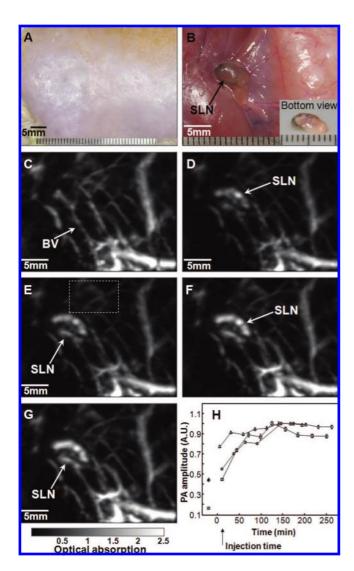
Figure 2. In vivo noninvasive photoacoustic time-course sagittal MAP images. (A) Photograph of axillary region with hair removed. (B) Photograph with skin and fatty tissue removed after the photoacoustic images had been recorded. The dark blue dyed lymphatic channel on the bottom of the SLN is shown in the inset. Photoacoustic images acquired before (C) and after (D–H) the nanocage injection: (D) 5 min (SLN started to appear), (E) 59 min, (F) 140 min, (G) 194 min. All images were acquired without signal averaging. (H) Accumulations of nanocages in a SLN over time, in terms of the amplitude changes of PA signals. After the injection, PA signals increased with time, which means gradual accumulations of nanocages. Peak accumulation occurred at ~140 min after the injection. PA signals from the SLN were normalized by those from adjacent blood vessels (the dotted box in Figure 2E) to minimize the ultrasonic focal effect, and normalized by maximum. Error bar is standard error. BV, blood vessels; SLN, sentinel lymph node. Color bar represents optical absorptions.

removal lotion before imaging. An intradermal injection of 0.1 mL of 2 nM Au nanocage solution was performed on a left forepaw pad.[35] During all image acquisitions, anesthesia was maintained using vaporized isoflurane (1 L/min oxygen and 0.75% isoflurane, Euthanex Corp.), and vitals were monitored using a pulseoximeter (NONIN Medical INC., 8600V). During the image acquisition, 8 mL of 0.9% saline was administered for hydration. After the image acquisition, the animals were euthanized by pentobarbital overdose. All
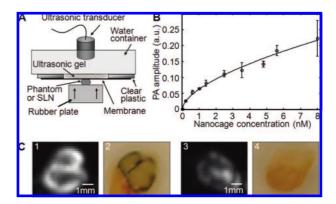
Figure 3. (A) Experimental setup for PA signal measurements from SLNs and gelatin phantoms containing nanocages. (B) PA signal from the gelatin phantom containing nanocages with various concentrations (0–8 nM). All measured values were scaled down to 0 dB gain. Errorbar indicates standard deviation. (C) Ex vivo photoacoustic images and photographs of dissected SLNs containing Au nanocages for PA signal measurement. A photoacoustic image (1) and a corresponding photograph (2) of the highly accumulated SLN. A photoacoustic image (3) and a corresponding photography (4) of the low accumulated SLN. In the photographs, dark blue represents the accumulation of nanocages. SLN, sentinel lymph node.

animal experiments were carried out in compliance with the guidelines on the care and use of laboratory animals at Washington University in St. Louis.

Results and Discussion. In a rat, an in vivo SLN containing Au nanocages was noninvasively imaged using the reflection-mode photoacoustic imaging system. Figure 2A shows a photograph of the axillae of the rat with hair removed before PA imaging. Figure 2B is a photograph of the same region with skin and fatty tissue removed, exposing the SLN containing Au nanocages after all PA images had been captured. The inset shows the bottom of the SLN, indicating the accumulated Au nanocages at its boundary. The size of the oval SLN was 4 mm × 6 mm. Before the injection of Au nanocages in the forepaw pad, a PA image was acquired as a control (Figure 2C). The vasculature within ~3 mm below the skin surface was displayed in the form of a maximum amplitude projection (MAP).[36] For visibility, PA signals beyond the 3 mm depth were excluded in the image formation. After the injection of Au nanocages (2 nM and 0.1 mL), scanning started immediately to evaluate the migration and accumulation time of the Au nanocages. PA signals from the SLN were detectable at about 5 min after the injection (Figure 2D). Here, the SLN was imaged with low contrast, implying low accumulation of Au nanocages at this time. Figures 2E–G show PA sagittal MAP images acquired at 54, 135, and 189 min after the injection, respectively. As time went by, the contrast at the SLN gradually increased, which means that more Au nanocages were gradually accumulated by the SLN.

To evaluate time-dependent changes in Au nanocage accumulation, the averaged values of the PA signal amplitudes within the SLN were calculated. To minimize the off-focus effect of an ultrasonic transducer in the PA signal measurement, the calculated PA values were normalized by those from the adjacent blood vessel, indicated by the dot-

ted box in Figure 2E. Figure 2H shows the variation of accumulation in terms of PA signal amplitude versus the time after injection. The peak accumulation time of Au nanocages in the SLN was observed to be about 140 min after the injection.

To estimate the concentration of Au nanocages accumulated in a SLN ex vivo, phantom experiments were conducted. The concept of this estimation is to compare PA signals from known-concentration phantoms with those from real SLNs. PA signals were obtained from the phantoms with the method described in Figure 3A. To reduce the propagation error of ultrasonic waves caused by different shapes, phantoms were slightly squeezed and flattened. The measured PA signals were plotted in Figure 3B as a function of concentrations.

Eight SLNs from four rats were harvested at about 150 min after the injection to estimate the concentrations of Au nanocages in real SLNs. In Figure 3C, ex vivo PA MAP images (1 and 3) and photographs (2 and 4) of two out of eight SLNs are shown as the examples. Figures 3C, 1 and 2 correspond to the SLN with highly accumulated Au nanocages. Figures 3C, 3 and 4 show the SLN with less accumulated Au nanocages. We measured PA signals from the eight real SLNs and derived the corresponding concentrations from Figure 3B. Five out of eight SLNs generated 0.2 ± 0.02 [au] PA signals (standard deviation), which corresponds to a concentration of 6.9 ± 0.29 nM (standard deviation), higher than the concentration of the original solution by a factor of 3.5. As observed in Figures 3C, 1 and 2, the Au nanocages seemed to accumulate mostly in the subcapsular sinus of the node and not drain much to the trabecular sinus, which explains the function of the lymph node as a filter. Therefore, the estimated value indicates the concentration of the locally accumulated Au nanocages. The rest of the SLNs produced PA signals of 0.02 ± 0.003 [au] (standard deviation), which corresponds to a concentration of 0.15 ± 0.016 nM (standard deviation). The large variations in concentration of Au nanocage in the SLNs were thought to be related to the physiology of lymphatic systems, such as the rate of lymphatic flow,[37] intrinsic smooth muscle action,[38] and physical skeletal muscle movement.[39]

The SLNs of rats are located ~2 mm below the skin surface. In humans, the mean depth of SLNs is 12 ± 5 mm (standard deviation, from the top surface of SLNs to the skin surface).[23] Therefore, it is necessary to demonstrate the clinical depth capability of the imaging technique based on optical contrast enhancement by Au nanocages. Just as in the previous experiments, the axillary region of another rat was imaged as a control before the injection of Au nanocages (Figure 4A). Figure 4B shows a sagittal PA MAP image of a SLN situated ~2 mm below the surface, obtained at 28 min after the injection. With a layer of chicken breast tissue placed on top of the axillary surface of the rat, a PA image was acquired at 126 min after the injection. The total depth of the SLN was now 10 mm (Figure 4C). With the second layer of chicken breast tissue, an imaging depth of 21 mm was demonstrated by acquiring a PA image at 165 min (Figure 4D). With the third layer of chicken breast tissue, a
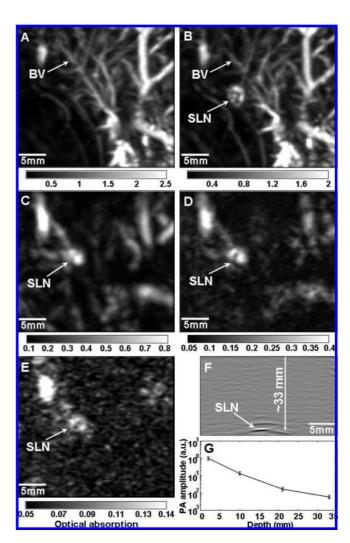

Figure 4. Depth capability of noninvasive photoacoustic SLN mapping in another rat, demonstrating potential for clinical use. Photoacoustic sagittal MAP images before (A) and after (B−E) the injection: (A) control image; (B) 28 min; (C) 126 min with a layer of chicken breast tissue placed on axillary region, total imaging depth was 10 mm; (D) 165 min with the second layer of chicken breast tissue, total imaging depth was 21 mm; (E) 226 min with the third layer of chicken breast tissue, total imaging depth was 33 mm. (F) Photoacoustic B-scan with 20 times signal average, showing the SLN located 33 mm deep. Memory of the acquisition system limited the record length in depth. (G) The amplitude variations of photoacoustic signals over imaging depths. Data were scaled down to 0 dB and normalized by the maximum. Errorbar represents standard deviation. All images were acquired without signal averaging except the B-scan (F). Colorbars represent the optical absorption. BV, blood vessel; SLN, sentinel lymph node.

PA image was obtained at 226 min after the injection (Figure 4E), and the total imaging depth reached 33 mm. In the B-scan image (Figure 4F), we averaged PA signals 20 times to improve the signal-to-noise ratio (SNR). With the signal averaging, the SNR was improved by about 7 dB. Figure 4G shows the amplitude changes of PA signals over imaging depths on a log scale. This plot represents the exponential decay of optical energy in tissues (neglect acoustic attenuation). It should be pointed out that all PA images in this study were acquired without signal averaging, except Figure 4F.

For future studies, several improvements concerning Au nanocages and the imaging system are recommended. First, an ideal mapping agent should be small enough to rapidly drain to lymphatic vessels and flow into lymph nodes but large enough to stay within the lymphatic system during the procedure. Particles smaller than 5 nm can leak into capillary blood vessels and flow into the cardiovascular circulatory system.[40,41] Once small particles (5−10 nm) drain to SLNs, they may quickly migrate to echelon lymph nodes; hence, they will increase the false positive rate. On the other hand, particles larger than 1000 nm mostly stay in the extracellular space (injection site). The Au nanocages that we used for this study had the average edge length of 50 nm, and the peak accumulation time was observed to be about 140 min. Even though the relationship between size and migration time for a certain shape was reported,[17] this will depend upon the shapes as well as the sizes of the tracers. Therefore, it is necessary to find an optimal size of Au nanocages for SLN mapping to secure fast migration, sufficient duration of trapping for imaging, and sufficiently strong PA signal generation for imaging deep sites. Second, even though various kinds of nanoparticles have widely been studied for biomedical applications, their potential toxicity currently limits their clinical use. For this study, we were not able to investigate the distribution of Au nanocages in a rat due to technical limitations. Unlike quantum dots,[24] Au-based nanoparticles do not have problems with heavy metal toxicity. Moreover, gold has been approved and used for human treatment.[24,42]

We observed a higher concentration accumulated in the subcapsular sinus of a SLN than the original solution of Au nanocages, but did not observe a solid trend of their clearance in the duration of measurement (up to 5 h). For SLN mapping, the higher accumulation would be beneficial, allowing a greater imaging depth with sufficient SNR. However, the higher accumulation and prolonged stay of Au nanocages may increase the chance of potential toxicity. Size adjustment and PEGylation of Au nanocages might reduce this prolonged stay,[43] so Au nanocages may be more efficiently excreted from the kidney.[17]

Another concern is the minimum detectable dose of Au nanocages in this PA system. For the SLN mapping, 0.1 mL of 2 nM Au nanocages solution was intradermally administered into the forepaw pad. The estimated concentration of the accumulated Au nanocages in the SLN was about 7 nM, which corresponded to ~22 dB SNR without signal averaging at 33 mm depth. In theory, the dose can be minimized until the SNR reaches the detection limit of the system. At 33 mm depth, the detection limit of the system was about 10 dB, which corresponded to ~0.05 [a.u.] in PA amplitude and ~0.67 nM in concentration. If Au nanocage accumulation in a SLN has a linear relationship with the dose, the minimum dose will be around 0.2 nM.

The last concern is that since the PA imaging system for this study employed a spherically focused ultrasonic transducer and a 10 Hz pulse-repetition-rate laser system, the scanning time for a 3D image was ~25 min with 0.2 mm and 0.35 mm stepsizes. In addition, the system was designed to sit on a table. The slow imaging speed and the tabletop design may not allow the imaging system to be directly applied in clinic. Employing an ultrasonic array system and a higher pulse-repetition-frequency laser system can dramatically improve the scanning time and flexibility of the scanner.

Conclusion. We have successfully accomplished noninvasive in vivo Au nanocage-contrast-enhanced SLN identification using PA imaging modality in a rat model. Compared to the conventional SLN mapping methods, the Au nanocages-based PA method offers several advantages: (1) noninvasive mapping, (2) peak optical absorption in the NIR region, allowing deeper imaging penetration than in the visible range, (3) rapid drainage into lymphatic channels, (4) accumulation of Au nanocages in excess of the original concentration, generating stronger PA signals (high SNR), (5) good spatial resolution, and (6) low cost. To evaluate this technique for clinical use, we also demonstrated that the proposed method could reach as deep as 33 mm below the skin surface with good contrast. This depth is greater than the mean depth of SLNs in human beings. Once Au nanocages are approved by the FDA, the next step will be a pilot study on human beings. In addition, with the aid of bioconjugation with antibodies for specific cancer cells the Au nanocage-based method can potentially provide noninvasive SLNB, while allowing simultaneous SLN identification.

References

(1) Sahoo, S. K.; Labhasetwar, V. *Drug Discovery Today* **2003**, *8* (24), 1112–20.

(2) Panyam, J.; Labhasetwar, V. *Adv. Drug Delivery Rev.* **2003**, *55* (3), 329–47.

(3) True, L. D.; Gao, X. *J. Mol. Diagn.* **2007**, *9* (1), 7–11.

(4) Gao, X.; Cui, Y.; Levenson, R. M.; Chung, L. W.; Nie, S. *Nat. Biotechnol.* **2004**, *22* (8), 969–76.

(5) Winter, P. M.; Caruthers, S. D.; Kassner, A.; Harris, T. D.; Chinen, L. K.; Allen, J. S.; Lacy, E. K.; Zhang, H.; Robertson, J. D.; Wickline, S. A.; Lanza, G. M. *Cancer Res.* **2003**, *63* (18), 5838–43.

(6) Harisinghani, M. G.; Barentsz, J.; Hahn, P. F.; Deserno, W. M.; Tabatabaei, S.; van de Kaa, C. H.; de la Rosette, J.; Weissleder, R. *N. Engl. J. Med.* **2003**, *348* (25), 2491–9.

(7) Kim, S.; Lim, Y. T.; Soltesz, E. G.; De Grand, A. M.; Lee, J.; Nakayama, A.; Parker, J. A.; Mihaljevic, T.; Laurence, R. G.; Dor, D. M.; Cohn, L. H.; Bawendi, M. G.; Frangioni, J. V. *Nat. Biotechnol.* **2004**, *22* (1), 93–97.

(8) Wang, Y. W.; Xie, X. Y.; Wang, X. D.; Ku, G.; Gill, K. L.; O'Neal, D. P.; Stoica, G.; Wang, L. V. *Nano Lett.* **2004**, *4* (9), 1689–1692.

(9) Kobayashi, H.; Brechbiel, M. W. *Curr. Pharm. Biotechnol.* **2004**, *5* (6), 539–49.

(10) Heesakkers, R. A.; Hovels, A. M.; Jager, G. J.; van den Bosch, H. C.; Witjes, J. A.; Raat, H. P.; Severens, J. L.; Adang, E. M.; van der Kaa, C. H.; Futterer, J. J.; Barentsz, J. *Lancet Oncol.* **2008**, *9* (9), 850–6.

(11) Harisinghani, M. *Lancet Oncol.* **2008**, *9* (9), 814–5.

(12) Rabin, O.; Manuel Perez, J.; Grimm, J.; Wojtkiewicz, G.; Weissleder, R. *Nat. Mater.* **2006**, *5* (2), 118–22.

(13) Hovels, A. M.; Heesakkers, R. A.; Adang, E. M.; Jager, G. J.; Barentsz, J. O. *Eur. Radiol.* **2004**, *14* (9), 1707–12.

(14) Morton, D. L.; Wen, D. R.; Wong, J. H.; Economou, J. S.; Cagle, L. A.; Storm, F. K.; Foshag, L. J.; Cochran, A. J. *Arch. Surg.* **1992**, *127* (4), 392–9.

(15) Krag, D. N.; Weaver, D. L.; Alex, J. C.; Fairbank, J. T. *Surg. Oncol.* **1993**, *2* (6), 335–9, discussion 340.

(16) Koyama, Y.; Talanov, V. S.; Bernardo, M.; Hama, Y.; Regino, C. A.; Brechbiel, M. W.; Choyke, P. L.; Kobayashi, H. *J. Magn. Reson. Imaging* **2007**, *25* (4), 866–71.

(17) Nakajima, M.; Takeda, M.; Kobayashi, M.; Suzuki, S.; Ohuchi, N. *Cancer Sci.* **2005**, *96* (6), 353–356.

(18) Oyen, R. H.; Van Poppel, H. P.; Ameye, F. E.; Van de Voorde, W. A.; Baert, A. L.; Baert, L. V. *Radiology* **1994**, *190* (2), 315–22.

(19) Saini, S.; Sharma, R.; Baron, R. L.; Turner, D. A.; Ros, P. R.; Hahn, P. F.; Small, W. C.; Delange, E. E.; Stillman, A. E.; Edelman, R. R.; Runge, V. M.; Outwater, E. K. *Clin. Radiol.* **2000**, *55* (9), 690–5.

(20) Michel, S. C.; Keller, T. M.; Frohlich, J. M.; Fink, D.; Caduff, R.; Seifert, B.; Marincek, B.; Kubik-Huch, R. A. *Radiology* **2002**, *225* (2), 527–36.

(21) Torchia, M. G.; Nason, R.; Danzinger, R.; Lewis, J. M.; Thliveris, J. A. *J. Surg. Oncol.* **2001**, *78* (3), 151–6, discussion 157.

(22) Parungo, C. P.; Colson, Y. L.; Kim, S. W.; Kim, S.; Cohn, L. H.; Bawendi, M. G.; Frangioni, J. V. *Chest* **2005**, *127* (5), 1799–1804.

(23) The depth of SLNs were measured by auxillary ultrasonography.

(24) Cuenca, A. G.; Jiang, H.; Hochwald, S. N.; Delano, M.; Cance, W. G.; Grobmyer, S. R. *Cancer* **2006**, *107* (3), 459–66.

(25) Song, K. H.; Stein, E. W.; Margenthaler, J. A.; Wang, L. V. *J. Biom. Opt.*, **2008**, *13* 5, 054033.

(26) Ku, G.; Wang, L. V. *Opt. Lett.* **2005**, *30* (5), 507–9.

(27) Sohrabnezhad, S.; Pourahmad, A.; Sadjadi, M. A. *Mater. Lett.* **2007**, *61* (11−12), 2311–2314.

(28) Skrabalak, S. E.; Chen, J.; Au, L.; Lu, X.; Li, X.; Xia, Y. *Adv. Mater.* **2007**, *19* (20), 3177–3184.

(29) Chen, J.; Saeki, F.; Wiley, B. J.; Cang, H.; Cobb, M. J.; Li, Z. Y.; Au, L.; Zhang, H.; Kimmey, M. B.; Li, X.; Xia, Y. *Nano Lett.* **2005**, *5* (3), 473–7.

(30) Hu, M.; Chen, J. Y.; Li, Z. Y.; Au, L.; Hartland, G. V.; Li, X. D.; Marquez, M.; Xia, Y. N. *Chem. Soc. Rev.* **2006**, *35* (11), 1084–1094.

(31) Sun, Y.; Xia, Y. *J. Am. Chem. Soc.* **2004**, *126* (12), 3892–901.

(32) Skrabalak, S. E.; Au, L.; Li, X. D.; Xia, Y. *Nat. Protoc.* **2007**, *2* (9), 2182–2190.

(33) Song, K. H.; Wang, L. V. *J. Biomed. Opt.* **2007**, *12* (6), 060503.

(34) *American National Standard for the Safe Use of Lasers: ANSI Z136.1− 2000.* American National Standards Institute: New York, 2000.

(35) Yang, X.; Skrabalak, S. E.; Li, Z. Y.; Xia, Y.; Wang, L. V. *Nano Lett.* **2007**, *7* (12), 3798–802.

(36) Song, K. H.; Wang, L. V. *J. Biomed. Opt.* **2007**, *12* (6), 060503.

(37) Uren, R. F.; Howman-Giles, R. B.; Thompson, J. F. *Ann. Surg. Oncol.* **1998**, *5* (6), 517–21.

(38) Moghimi, S. M.; Bonnemain, B. *Adv. Drug Delivery Rev.* **1999**, *37* (1−3), 295–312.

(39) Ikomi, F.; Hunt, J.; Hanna, G.; Schmid-Schonbein, G. W. *J. Appl. Physiol.* **1996**, *81* (5), 2060–7.

(40) Alazraki, N. P.; Eshima, D.; Eshima, L. A.; Herda, S. C.; Murray, D. R.; Vansant, J. P.; Taylor, A. T. *Semin. Nucl. Med.* **1997**, *27* (1), 55–67.

(41) Soltesz, E. G.; Kim, S.; Laurence, R. G.; DeGrand, A. M.; Parungo, C. P.; Dor, D. M.; Cohn, L. H.; Bawendi, M. G.; Frangioni, J. V.; Mihaljevic, T. *Ann. Thorac. Surg.* **2005**, *79* (1), 269–77.

(42) Mottram, P. L. *Immunol. Cell. Biol.* **2003**, *81* (5), 350–3.

(43) Otsuka, H.; Nagasaki, Y.; Kataoka, K. *Adv. Drug Delivery Rev.* **2003**, *55* (3), 403–19.

NL802746W